Author(s): Mattsson, Ida; Lahtinen, Manu; Sitdikov, Ruzal; Wank, Bianca; Saloranta-Simell, Tiina; Leino, Reko

Title: Phase-selective low molecular weight organogelators derived from allylated D-mannose

Year: 2022

Version: Published version

Please cite the original version:

Mattsson, I., Lahtinen, M., Sitdikov, R., Wank, B., Saloranta-Simell, T., & Leino, R. (2022). Phase-selective low molecular weight organogelators derived from allylated D-mannose. Carbohydrate research, 518, Article 108596. https://doi.org/10.1016/j.carres.2022.108596

Carbohydrate Research 518 (2022) 108596

Contents lists available at ScienceDirect

Carbohydrate Research

journal homepage: www.elsevier.com/locate/carres

Phase-selective low molecular weight organogelators derived from allylated D-mannose

Ida Mattsson [a], Manu Lahtinen [b], Ruzal Sitdikov [a], Bianca Wank [a], Tiina Saloranta-Simell [a], Reko Leino [a,*]

[a] Laboratory of Molecular Science and Engineering, Åbo Akademi University, 20500, Turku, Finland
[b] Department of Chemistry, University of Jyväskylä, Jyväskylä, FI-40014, Finland

ARTICLE INFO

Keywords:
LMWOG
Gels
D-mannose
Phase selectivity
Solid state NMR spectroscopy

ABSTRACT

In the last decades, synthesis and design of low molecular weight organogelators has gained increasing attention due to their versatile use in, for example, cosmetics, biomedicine and oil spill remediation. In this work, three potential gelators have been prepared from allylated D-mannose. Both the gelators and the corresponding gels formed were thoroughly characterized by crystallography, FTIR spectroscopy, SEM, rheometry and NMR spectroscopy, in solution and in solid state. The results showed that two of the compounds phase-selectively form gels with hydrocarbon solvents. The most promising gelator compound is alkene terminated, with the unsaturated end functionality not critical for gel formation, tentatively providing the possibility for customizing the gelation properties by further chemical modification. Alternatively, the alkene group could possibly be utilized as a linker for future coupling to carrier materials or surfaces to further increase the mechanical strength of the gel.

1. Introduction

Recent decades have witnessed a steadily increasing interest in the design and preparation of low-molecular weight organogelators (LMWOGs), in particular based on carbohydrates [1]. The attention to these compounds originates from their many potential applications in, for example, cosmetics [2,3], biomedicine, including tissue engineering [4,5], and drug delivery materials [6], soft optical devices [7–10] and supramolecular electronic devices [11], as well as water purification applications [12–15]. LMWOGs are generally defined as organic compounds with molecular weights <1000 g/mol, able to immobilize different solvents by self-assembling into 3D networks of higher-ordered structures, such as fibrous, tubular or helical aggregates [16,17]. The self-assembly is mediated by non-covalent intermolecular interactions, including hydrogen-bonding, dipole-dipole interactions, π-π-stacking, electrostatic effects, van der Waals forces or solvophobic effects [18,19].

Organic molecules able to selectively gelate the organic phase of a binary solvent mixture are denoted phase selective gelators (PSGs). Such compounds have gained much attention as a potential remedy for oil spill recovery and water purification, with water pollution constituting a severe risk for the environment, in particular marine ecosystems. In earlier work, Bhattacharya and Krishnan-Ghosh have described a phase selective LMWOG derived from an alanine-based amphiphile, able to selectively solidify oil from an oil-water mixture [12]. Later, a range of molecular building blocks have been used for designing new phase selective organogelators. Due to their structural diversity, high abundance, low toxicity, biocompatibility and degradability, particularly carbohydrates have received substantial interest in the LMWOG field [20–22], with several phase selective carbohydrate-derived gelators having been reported in the literature [1,19–37]. Most of these, however, lack additional functional groups which do not participate in the gelation process. Such functionalities could, in principle, be used for covalent or non-covalent binding of the gelators to other materials, for example nanoparticles or surfaces, in order to improve their mechanical strength, stability and applicability of the resulting gels.

Inspired by the previously published mannitol-based LMWOG **1** [37], we have here investigated the gelation properties of structurally similar compounds **2**–**4** derived from allylated D-mannose (Fig. 1). In previous work, we have shown that such allylated mannose-derivatives form strong intermolecular hydrogen bond networks [38,39]. Earlier, in some studies, mannitol-derived gelator compounds have been shown to possess superior gelating properties in comparison to other sugar alcohols, such as sorbitol and xylitol [32].

For investigating the hydrophilic/hydrophobic ratio required for gel

* Corresponding author.
E-mail address: reko.leino@abo.fi (R. Leino).

https://doi.org/10.1016/j.carres.2022.108596
Received 11 March 2022; Received in revised form 10 May 2022; Accepted 17 May 2022
Available online 24 May 2022

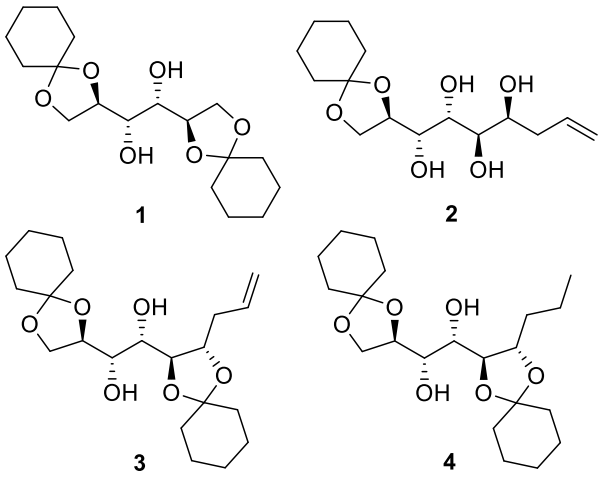

Fig. 1. Structures of the mannitol model compound 1 [37] and the organogelators 2–4 investigated in this work.

formation, alkene-terminated compounds **2** and **3**, bearing four and two free hydroxyl groups, respectively, were prepared (Fig. 1). Furthermore, for verifying that the alkene moiety is not critical for gel formation, thus being available for further chemical modification, also a saturated analogue of compound **3** (compound **4**, Fig. 1) was prepared. Here, we describe the synthesis and gelation testing of these potential LMWOGs derived from allylated D-mannose. The new compounds prepared and their corresponding gels were thoroughly characterized by NMR spectroscopy, in both solution and solid state, FTIR spectroscopy, single crystal X-ray diffraction (SCXRD), powder X-ray diffraction (PXRD), optical microscopy and SEM.

2. Results and discussion

2.1. Synthesis of gelator compounds

Allylated D-mannose and its hydrogenated congener were synthesized following previously published protocols [38,39]. The polyols were subsequently transformed to the gelator compounds **2**, **3** and **4** through acid catalyzed ketal formation in dry DMF under reduced pressure (Scheme 1). The reaction products, obtained as white powders, were purified by flash chromatography (for details, see ESI), albeit isolated in only poor to fair yields. The primary aim of the present work was mainly to elucidate the gelation properties of these compounds. However, for larger scale applications further optimization of the synthetic route is still needed.

2.2. Gelation studies

Gel formation studies showed that compounds **3** and **4** form gels with hydrocarbons and oils (Table 1). Compound **2** did not show gelation in any of the solvents tested and, consequently, was excluded from any further investigations in this work. The solubility of compound **2** in the hydrophobic solvents, gelated by compounds **3** and **4**, was low even at elevated temperatures. It appears that compound **2** is too polar, and the solvophobic effects become too pronounced for gelation to occur. Evidently, two cyclic ketals are required in these structures for gelation to take place. Results from the gelation studies with compounds **3** and **4** are summarized in Table 1. In the solvents where the gelator compounds **3** and **4** formed a gel, opaque gels were received upon cooling.

Table 1
Minimum gelation concentrations and T_{gel} of compounds **3** and **4** in various solvents.

Solvent	Compound 3		Compound 4	
	MGC[a]	T_{gel}[b]	MGC[a]	T_{gel}[b]
Pentane	Insol.[c]	–	Insol.[c]	–
Hexane	1.37	34	1.62	29
Heptane	1.33	38	1.53	32
Decane	1.25	47	1.30	38
Tetradecane	1.17	48	1.27	39
Cyclohexane	2	36	Sol.	–
Sunflower seed oil	2	41	Sol.	–
Mineral oil	1.33	44	1.67	43
Diesel	Cryst.[d]	–	Cryst.[d]	–
Gasoline (95E10)	Sol.[e]	–	Sol.[e]	–
Dichloro-methane	Sol.[e]	–	Sol.[e]	–
Chloroform	Sol.[e]	–	Sol.[e]	–
Methanol	Sol.[e]	–	Sol.[e]	–
Ethanol	Sol.[e]	–	Sol.[e]	–
Ethyl acetate	Sol.[e]	–	Sol.[e]	–
Toluene	Sol.[e]	–	Sol.[e]	–

[a] Minimum gelation concentration (% w/v, mg/ml).
[b] Gelation temperature (°C) obtained at 2% w/v.
[c] Insoluble even at solvent boiling point.
[d] Crystallizes instead of gel formation.
[e] Soluble even at 10% w/v.

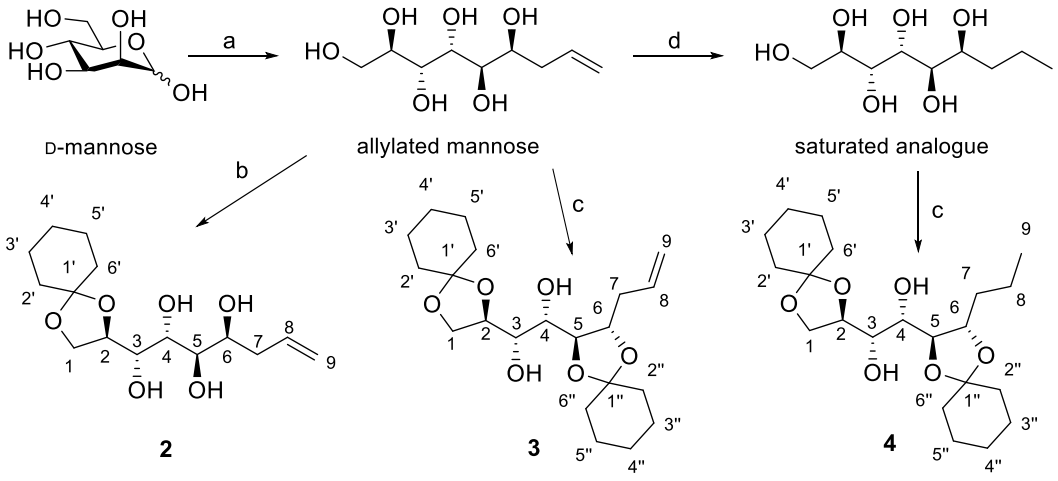

Scheme 1. Synthesis of the gelator compounds **2**–**4**. a) D-Mannose (1 eq.), tin powder (2 eq.), allyl bromide (3 eq.), EtOH:H_2O 10:1, 60 °C, overnight, 53% yield. b) Cyclohexanone dimethyl ketal (1.1 eq.), *p*-TSOH (0.1 eq), dry DMF, 200 mbar, 60 °C, 2 h, 48% yield. c) Cyclohexanone dimethyl ketal (2.1 eq.), *p*-TSOH (0.1 eq), dry DMF, 200 mbar, 60 °C, 2 h, 43–46% yield. d) H_2, 3 atm, 10% Pd/C, overnight, quant. yield.

Solubilities of **3** and **4** are poor in most hydrocarbon solvents at room temperature and, since dissolution of the compound is critical for gel formation, heating is typically required. All gels formed were stable to inversion at 2% w/v (Fig. 2). In all cases, the gelation process was thermoreversible, with the gels formed tolerating at least three heating-gelation cycles. Furthermore, the gels are stable at room temperature for at least three weeks. The organic phase can easily be recovered from the gelator by distillation and the gelators can subsequently be reused. Neither one of the gelator compounds **3** and **4** formed gels in dichloromethane, chloroform, methanol, ethanol, ethyl acetate or toluene, and the gelators were fully soluble in these solvents even at 10% w/v. Surprisingly, neither one of the compounds was able to gelate diesel or gasoline. In diesel, for reasons unknown, compounds **3** and **4** formed needle-like crystals instead, while both were fully soluble in gasoline. The inability to form gels in gasoline could possibly be explained by the standard grades of gasoline containing up to 10% v/v ethanol. The ethanol molecules may compete for hydrogen bonding and prevent the gelator molecules from forming the intermolecular hydrogen bond networks required for gel formation [37]. Adding small amounts of ethanol or methanol to solvents where the gelators otherwise form gels supports this theory, with the addition of alcohol disrupting the hydrogen bond network, subsequently also dissolving the gelator compound in the solvent mixture.

Some gelation experiments were also conducted in binary solvent mixtures. Both compounds **3** and **4** can selectively gelate the organic phase in water/hexane and water/decane mixtures. The 2% w/v gels of compound **3** in both hexane and decane are stable to inversion (Fig. 3), whereas only the decane gel of compound **4** was able to hold the weight of the water upon inversion, indicating that gelator **3** forms a mechanically stronger gel than compound **4**.

2.3. Rheological studies

Rheological analyses were conducted in order to compare the mechanical strength of the gels formed by compounds **3** and **4**, each 5% w/v in decane. From a rheological perspective, gels can be defined as two-component systems where the storage modulus (G′) is larger than the loss modulus (G″) with little to none frequency dependency of the moduli [30,40,41]. Amplitude sweep experiments showed that both gels exhibit typical gel behavior with G'>G″ at lower strains, but at higher strain the moduli cross and the behavior become more liquid or solution-like (Fig. 4). The intersection point of the two moduli, γ,

Fig. 2. Gels formed with compound **3** in: a) hexane; b) heptane; c) decane; d) tetradecane; e) cyclohexane; f) sunflower seed oil; and g) mineral oil (top). Gels formed with compound **4** in: h) hexane; i) heptane; j) decane; k) tetradecane; and l) mineral oil (bottom).

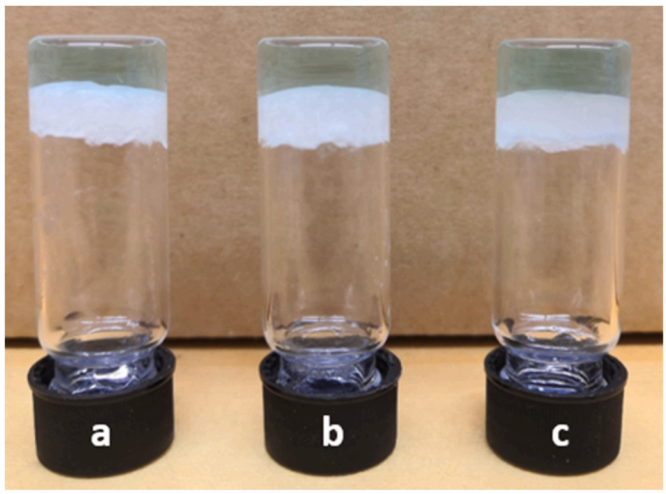

Fig. 3. Phase selective gelation of: a) compound **3** in water/hexane; b) compound **3** in water/decane mixture; and, c) compound **4** in water/decane mixture. Copper sulfate was added to the aqueous phase for improved visibility.

showed that the properties shift from gel-like to solution-like at similar strain, 3.403% for gelator **3** and 3.239% for gelator **4**, respectively. The G′ value of the linear region is, however, significantly higher for the gel composed of gelator **3** compared to gelator **4** (approx. 0.07 MPa vs. 0.02 MPa, respectively). Values for tan(δ), i.e., the ratio of G″ to G′, were obtained from the viscoelastic region of the frequency sweep experiments (Fig. 5). The values of tan(δ) are similar for the two gels, being 0.73 for gelator **3** and 0.74 for gelator **4**, respectively. The relatively high tan(δ) of the gels indicate that they are weak gels [42], but as they tolerate scooping and inversion, they could be practically useful for applications requiring only mild handling.

2.4. FTIR spectroscopic analysis

FTIR-ATR spectroscopic analyses were conducted on gelator compounds **3** and **4**, both on the bulk powders and 5% w/v gels in decane (Fig. 6). The FTIR spectra did not show any sharp signals at around 3600 cm-1, indicating that free hydroxyl groups exist neither in the bulk state nor in the gel. Instead, the broad signals at 3200 cm-1 to 3500 cm-1 suggest that all hydroxyl groups are involved in hydrogen bonding [43]. Consequently, it can be concluded that hydrogen bonding is the major force behind the self-assembly both in the gel form and the solid state of these compounds.

2.5. Crystallographic analysis

Single crystals of gelators **3** and **4** were obtained by recrystallization from hexane/ethyl acetate. Compound **3** crystallizes as colorless, long needles in a monoclinic crystal system and polar space group $P2_1$ with two molecules in the asymmetric unit (Fig. 7). The carbohydrate backbone adopts an L-shape with the allyl group at one end of the backbone. The intermolecular packing of the molecules in the crystal lattice are set by mutual O–H···O, hydrogen bonding (Table ESI1) between the OH groups (O41–H···O15, O17–H···O43, O15–H···O17 and O41–H···O43) of four adjacent molecules, forming a square-planar hydrogen bond network that arranges the molecules in paired rows extending along the *b*-axis in a parallel fashion (Fig. 7). In the structure, also slight disorder is observed on one of the cyclohexanone ketal groups per molecule in an asymmetric unit.

Compound **4**, likewise, crystallizes as long needles in a monoclinic crystal system but in space group *C*2 instead of $P2_1$. The asymmetric unit contains three separate molecules of which one shows disorder similar to compound **3** (Fig. 8). The molecular packing resembles compound **3**,

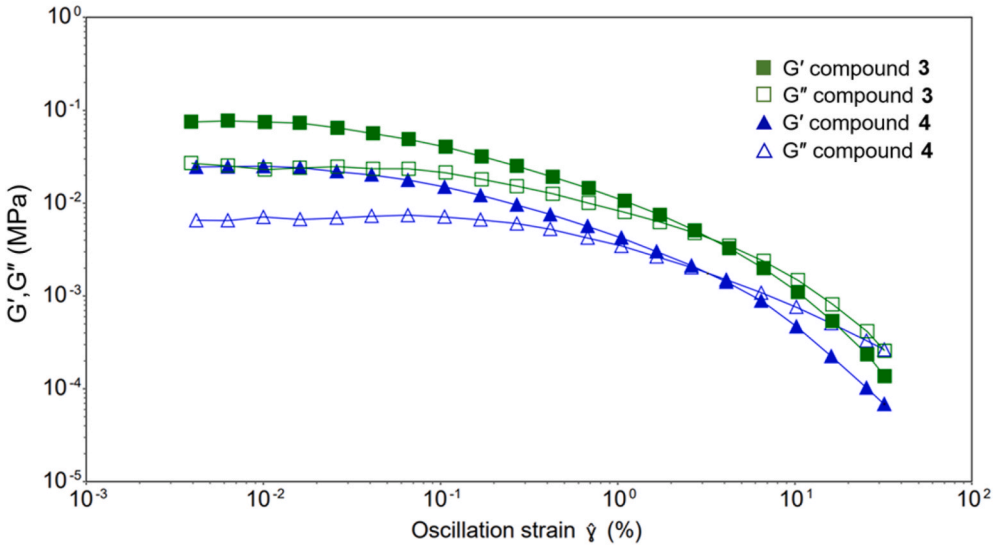

Fig. 4. Amplitude sweep for 5% w/v gels formed with compounds **3** and **4** in decane.

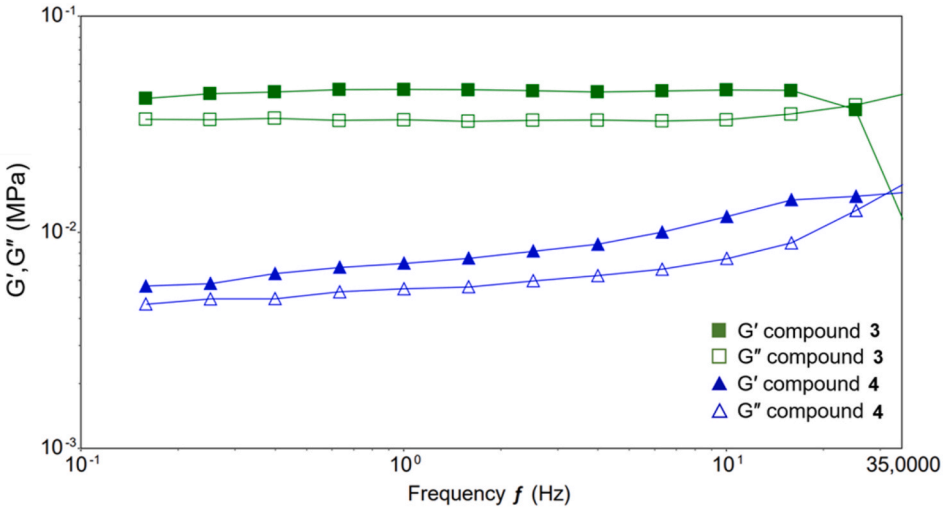

Fig. 5. Frequency sweep for 5% w/v gels formed with compounds **3** and **4** in decane.

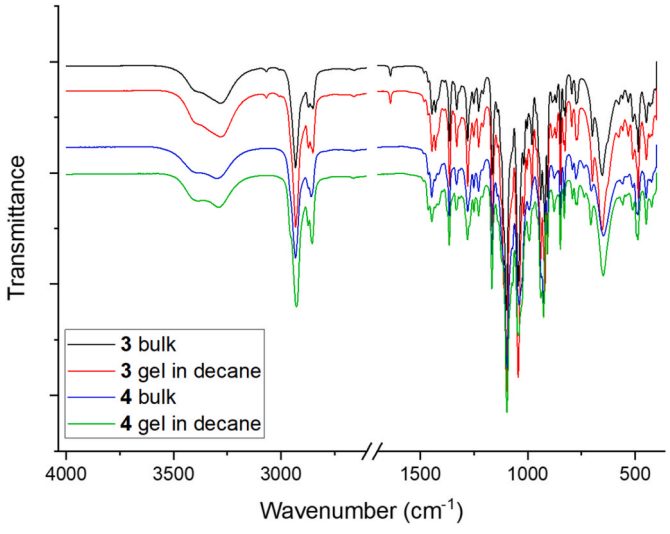

Fig. 6. FTIR-ATR spectra of compounds **3** and **4** in the bulk and gel forms.

having a similar packing scheme and hydrogen bonding network wherein the hydroxyl groups of adjacent and confronted molecules are bonded through hydroxyl groups (O15, O17, O42, O44, O69 and O71, see Table ESI2).

Next, powder diffraction analyses were performed to confirm the structural equivalence between the determined single crystal structures and the corresponding bulk powders, xerogels and native gels. As shown in Figure ESI1 and Figure ESI2, Pawley fits with the single crystal unit cells of **3** and **4** showed a good match between the experimental and calculated peak profiles, resulting in good line profile fitting factors (R_p and R_{wp}), as summarized in Table 2 (for full crystal data and refinement parameters, see Table ESI3). While the obtained single crystal data of compound **4** is of poor quality, the good Pawley fit together with the structural similarity to compound **3** supports the conclusions.

As shown by the thermo-microscope images displayed in Fig. 9, both gels **3** and **4** contain a large number of cross-grown long crystalline fibers along with a nearly opaque gel mass. The crystallinity of the fibers is evidenced by the images with the cross-polarized light, as well as by the fact that the measured PXRD patterns clearly showed characteristic diffraction peaks originating from the structural modification determined by the single-crystal X-ray diffraction in both cases. The pattern of

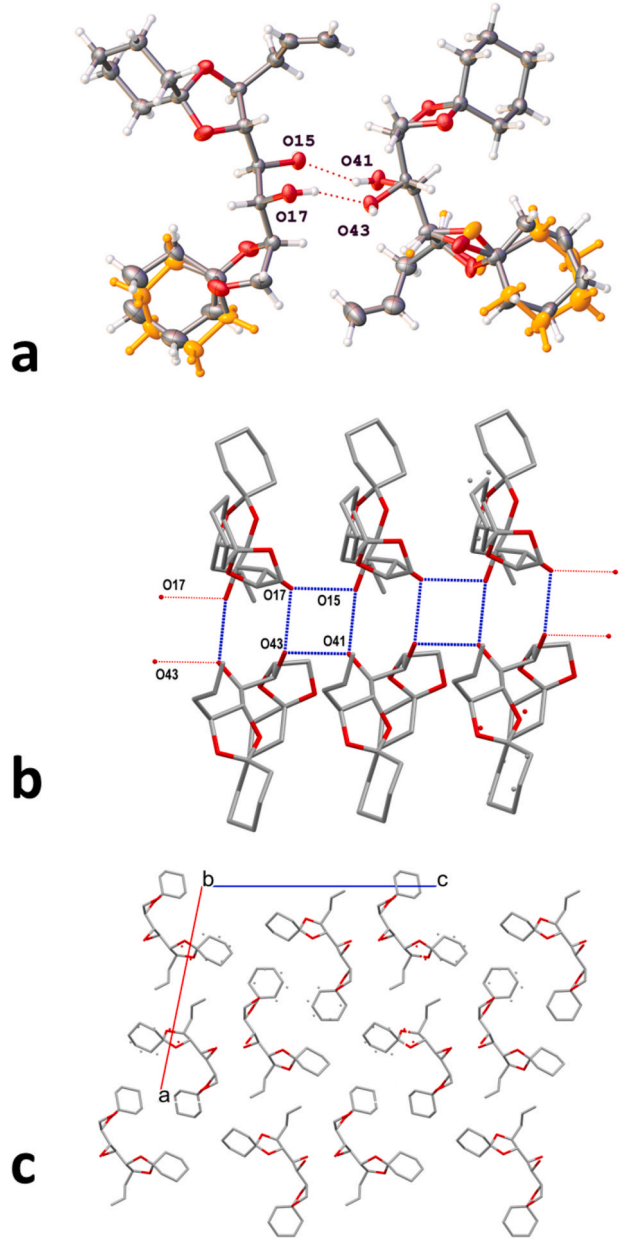

Fig. 7. a) Illustration of an asymmetric unit of the crystal structure of **3** with disordering of cyclohexanone ketal groups highlighted in orange color. b) Partial view of the square-planar hydrogen bonding network between the adjacent molecules (hydrogen bonds showed in dashed blue lines). c) Molecular packing along the *b*-axis. Thermal displacement ellipsoids are shown at the 50% probability level, and the hydrogen atoms have been removed from the packing images for the sake of the clarity.

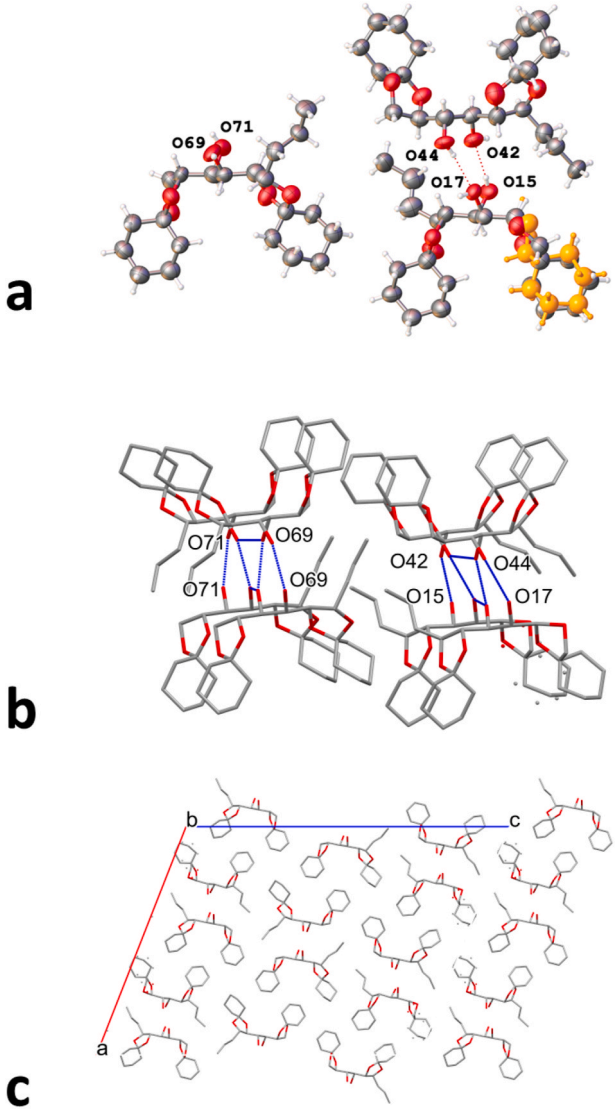

Fig. 8. a) Illustration of an asymmetric unit of the crystal structure of **4**. Disordered group is highlighted in orange color. b) Partial view of square-planar hydrogen bonding network between the adjacent molecules (hydrogen bonds shown in dashed blue lines). c) Molecular packing along the *b*-axis. Thermal displacement ellipsoids are shown at the 50% probability level, and the hydrogen atoms have been removed from the packing images for the sake of the clarity.

the native gels also show an extremely broad diffraction hump in the 2θ range of 12–26°, which originates from the nearly amorphous gel mass. The PXRD patterns of the air dried xerogels show that the amorphous content is lost, and has clearly crystallized back to the original structure matching with the pristine bulk powder, as well as the crystalline fibers already present in the native gels. The PXRD patterns of bulk powders, xerogels, and native gels (5% w/v in n-decane) of compounds **3** and **4** are shown in Figs. 10 and 11, respectively.

2.6. SEM analysis

In order to further visually examine the aggregation mode, a selection of the gels were subjected to SEM analysis. SEM images of xerogels of compound **3** obtained from hexane and cyclohexane, and compound **4** in hexane demonstrate that the gels consist of entangled networks of straw-like fibrillar structures (Fig. 12). The fibril-forming behavior is expected from carbohydrate-derived organogelators [44]. The thermoreversible self-assembly generates fibers which prevent the flow by immobilizing the solvent within the three-dimensional network. Compound **3** displays fibrillar structures of 0.3–0.9 μm in diameter and >100 μm in length in hexane. The corresponding gel in cyclohexane consists of slightly larger fibers (Ø 0.3–1.3 μm, length >100 μm). These fibers appear more prone to forming bundles than the analogous gel from hexane, with the SEM images also showing the occurrence of short (3–5 μm) fibrillary fragments. The formation of bundles and short fragments of fibers might explain why gelator **3** has higher MGC in cyclohexane than in hexane, as the immobilization of the solvent may be less efficient by bundles than by more well separated fibers. Diameters of the fibers formed in hexane by gelator **4** range from 0.3 to 1.3 μm. The length of the fibers is also in this case generally >100 μm. It should again

Table 2
Crystal data and for compounds **3** and **4** (full listing in Table ESI1).

Compound	3		4	
Method	SCXRD	PXRD	SCXRD	PXRD
Empirical formula	$C_{21}H_{34}O_6$	$C_{21}H_{34}O_6$	$C_{21}H_{36}O_6$	$C_{21}H_{36}O_6$
Formula weight	382.48	382.48	384.50	384.50
Temperature (K)	120.01 (10)	295 (1)	120.01 (10)	295 (1)
Crystal system	monoclinic	monoclinic	monoclinic	monoclinic
Space group	$P2_1$	$P2_1$	$C2$	$C2$
a (Å)	19.1173 (6)	19.407 (3)	31.173 (3)	31.25 (2)
b (Å)	5.45290 (10)	5.501 (1)	5.3975 (4)	5.320 (6)
c (Å)	20.3454 (7)	20.659 (3)	41.089 (3)	41.10 (2)
α (°)	90	90	90	90
β (°)	101.453 (3)	102.570 (1)	111.426 (10)	111.453 (5)
γ (°)	90	90	90	90
Volume (Å^3)	2078.67 (11)	2152.64	6435.6 (10)	6359.56
Final R indexes [I ≥ 2σ (I)]	$R_1 = 0.0459$, $wR_2 = 0.0954$	$R_p = 0.0453$[a] $R_{wp} = 0.0565$[a]	$R_1 = 0.1524$, $wR_2 = 0.3377$	$R_p = 0.0741$[a] $R_{wp} = 0.0941$[a]
Final R indexes (all data)	$R_1 = 0.0691$, $wR_2 = 0.1041$		$R_1 = 0.3616$, $wR_2 = 0.5084$	
Largest diff. Peak/hole/e (Å^{-3})	0.24/-0.17		0.47/-0.34	
Flack parameter	0.08 (13)		0.1 (6)	

[a] R_p and R_{wp} = R-factors for profile and weighted profile, respectively.

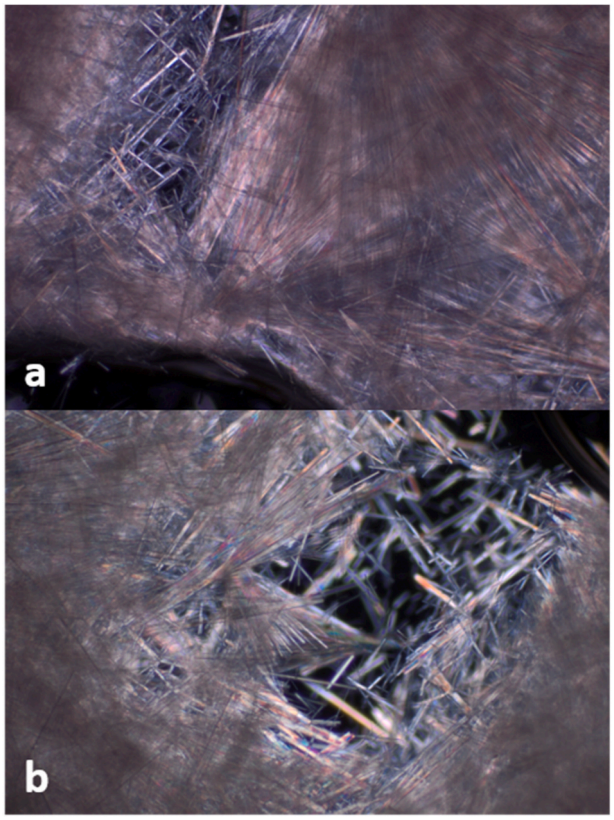

Fig. 9. Thermo-microscope images of 5% w/v gels of a) compound **3** in decane, and b) compound **4** in decane. Images were obtained at 25 °C with 50X magnification.

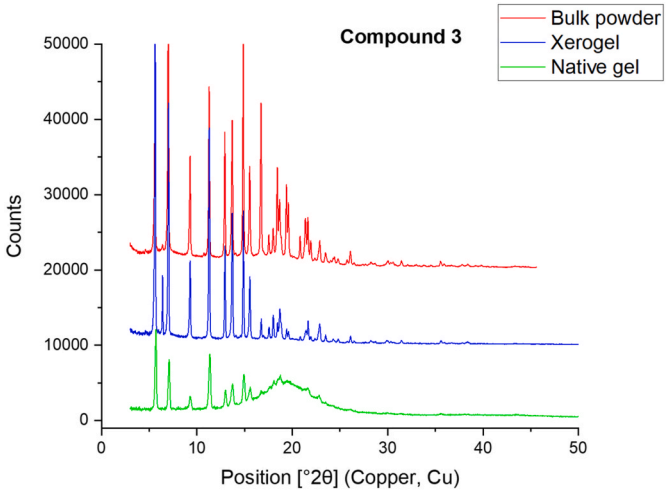

Fig. 10. PXRD patterns of the bulk powder, xerogel and native gel (5% w/v in decane) of compound **3**.

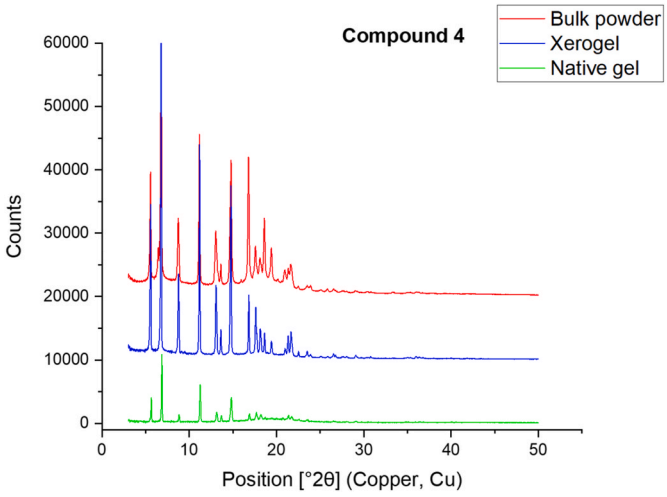

Fig. 11. PXRD patterns of the bulk powder, xerogel and native gel (5% w/v in decane) of compound **4**.

be noted, however, that the morphological structure of the xerogel may not be fully representative of the structure of the native gel.

2.7. NMR spectroscopic analysis

In addition to FTIR and crystallographic methods, NMR spectroscopy is a valuable tool for providing further insight on the intermolecular forces involved in the self-assembly taking place during gel-formation. In fact, solution state NMR experiments have been extensively used for both understanding the interactions involved in the self-assembly processes associated with gelation, as well as for gaining information about the self-assembling structures under various stages of gelation [45–50]. According to some reports, it is believed that the gels exist in equilibrium between the aggregated and non-aggregated forms of the gelator molecules [50]. The appearance of additional, separate signals in the gel form, compared to the solution form of the gelator molecules, would then indicate that the chemical exchange between the self-assembled and non-self-assembled species is slow on the NMR timescale. Fast chemical exchange would, on the contrary, not give rise to new signals in the gel form [44,51]. Thus, the well-resolved signals observed in the ^{1}H NMR spectra of the gels would originate from the non-associated gelator molecules, whereas the aggregated structures

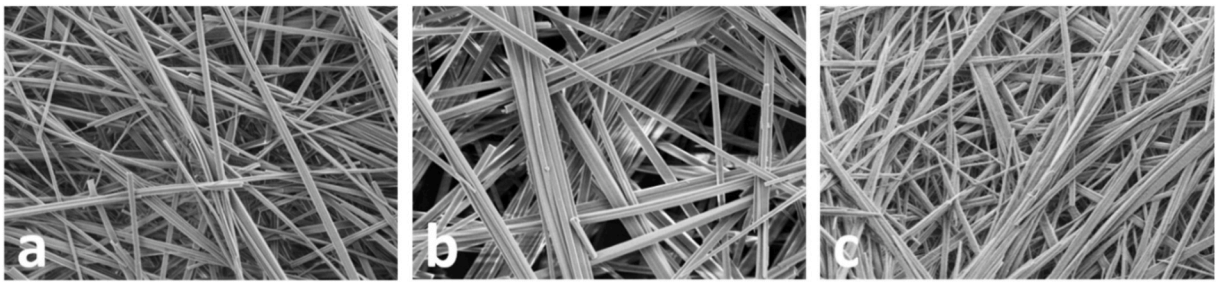

Fig. 12. SEM images of the xerogels of a) Compound **3** in hexane; b) Compound **3** in cyclohexane; c) Compound **4** in hexane. Magnification X2.5k.

would instead be NMR silent [45,48]. Other reports, however, speculate that the well resolved signals instead would originate from the mobile parts of the gel fibers [49].

^{1}H NMR experiments were conducted in order to additionally confirm that the driving forces behind the gel formation involve hydrogen bonding. Variable concentration (VC) ^{1}H NMR experiments were first conducted by changing the concentration of the gelator from 0.2 to 2% w/v in decane-d_{22}. More gelator was gradually added to increase the concentration. After every addition, the sample was heated in order for the gelator compound to dissolve. The spectra were recorded immediately when the sample temperature had reached 25 °C. Upon increasing the concentration of both gelators **3** and **4**, the signals from the hydroxyl groups gradually shifted downfield, which generally is indicative of the formation of strong intermolecular hydrogen bonds (Figs. 13 and 14) [43].

In the case of gelator **3**, some signals in the carbohydrate region slightly shift downfield (Figure ESI3). The allyl protons, however, remained at the same chemical shift throughout the series of concentration increase, suggesting that the allylic protons do not participate in the intermolecular interactions involved in promoting the gel formation. The ^{1}H NMR spectrum of gelator **4** at 2% w/v shows some splitting of the OH signals, consistent with the occurrence of more than one NMR visible species (Fig. 14, for zoomed in image, see Figure ESI4).

Variable temperature (VT) ^{1}H NMR experiments were also conducted by recording the spectra of 2% w/v gel in decane-d_{22} which had been allowed to set overnight. The variable temperature experiments were recorded from 25 to 65 °C and back from 65 to 25 °C, in 10 °C intervals. The temperature was allowed to stabilize for 20 min before recording the spectrum. It became evident immediately that the spectra recorded at 2% w/v concentration in the VC NMR spectroscopic experiments looked very different from the spectra recorded at the same concentration where the sample had been allowed to set overnight. In the spectra of gelator **3**, several new broad and poorly resolved signals appear (Fig. 15, for the full spectra, see Figure ESI5). The appearance of the new signals indicates that at least a fraction of the self-assembled species is not NMR silent and that both associated and non-associated species can be observed by ^{1}H NMR spectroscopy.

Upon heating of the gelator **3** sample, the spectra became better resolved and the OH signals shifted upfield, as expected when the intermolecular hydrogen bonds become weaker (Fig. 15). At 65 °C, the spectrum of compound **3** resembles the data recorded at sub-gelation concentrations, i.e., solution spectra (see ESI). Upon cooling, the OH signals again migrate downfield when the intermolecular hydrogen bond network re-forms. ^{1}H NMR spectra recorded at the same temperature upon heating and cooling appear similar, indicating that 20 min is sufficient for the system to equilibrate or stabilize at a certain temperature (Fig. 15).

In the ^{1}H NMR spectrum of gelator **4** no new signals appeared when

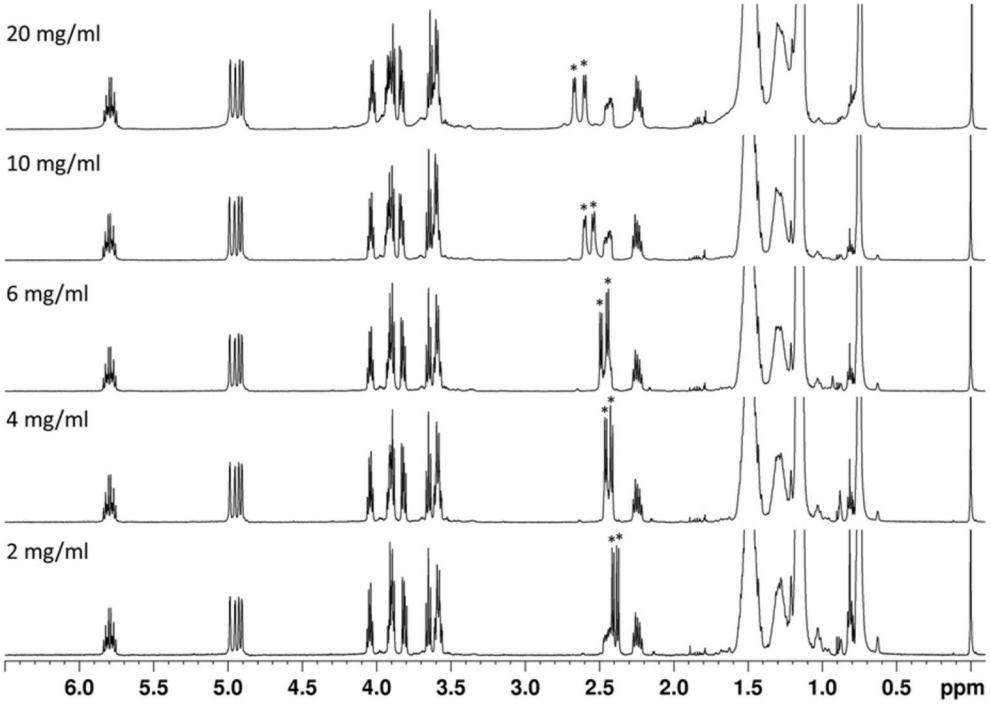

Fig. 13. Variable concentration ^{1}H NMR spectra of compound **3** in decane-d_{22}. The signals originating from the hydroxyl groups are denoted by *.

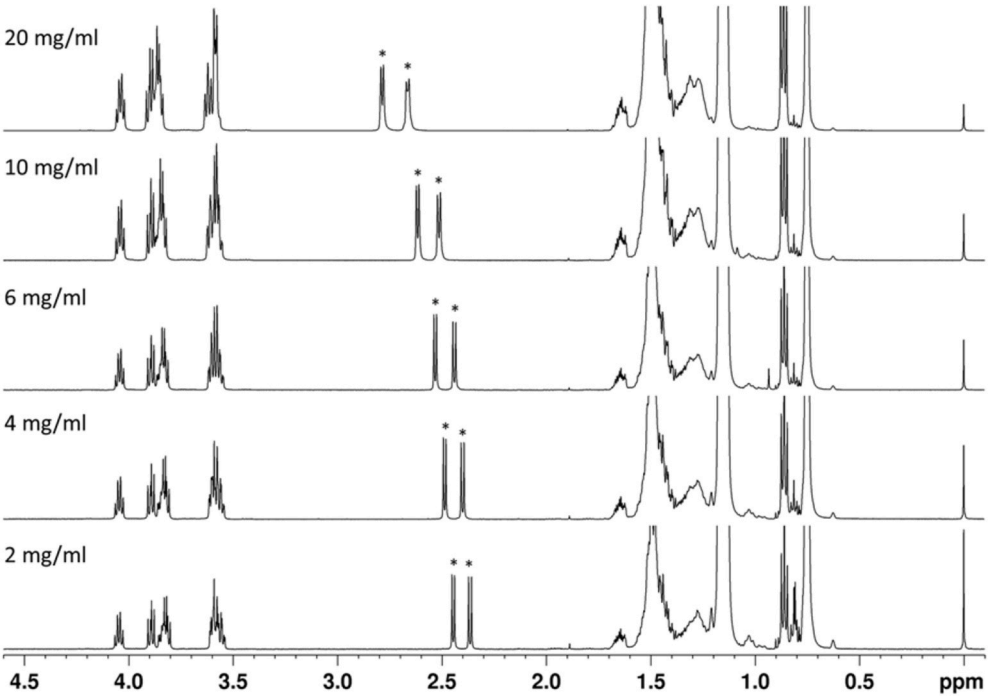

Fig. 14. Variable concentration ^{1}H NMR spectra of compound **4** in decane-d_{22}. The signals originating from the hydroxyl groups are denoted by *.

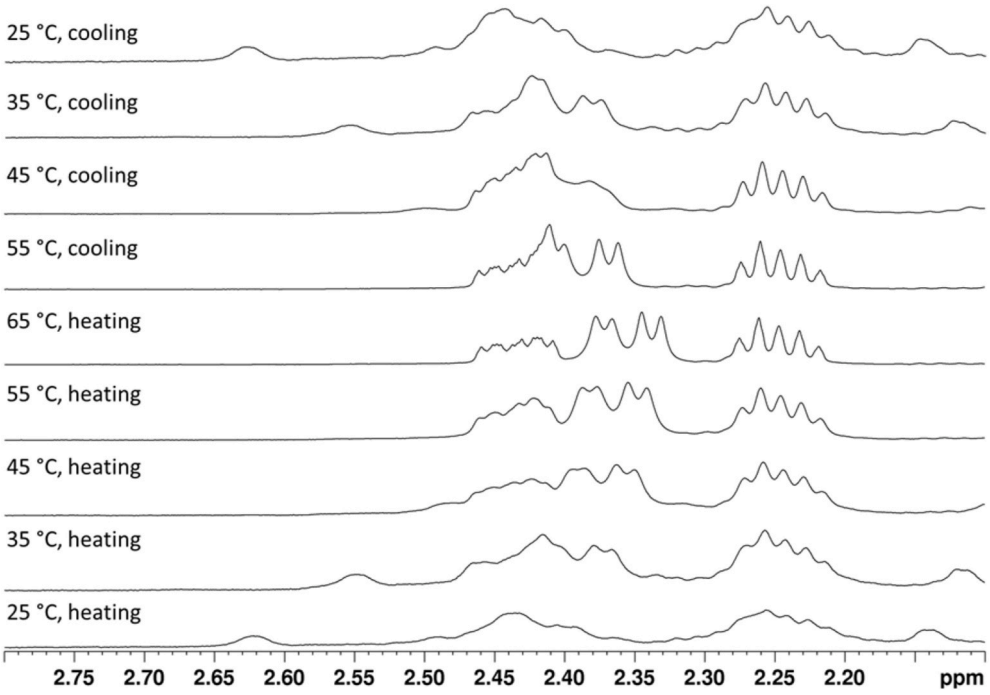

Fig. 15. Variable temperature ^{1}H NMR spectra (selected region for clarity) of compound **3** in decane-d_{22}.

the 2% w/v gel in decande-d_{22} was allowed to set overnight, indicating that the associated species might be NMR silent. The OH signals had, however, shifted upfield compared to the spectrum of the same concentration recorded immediately after the heated solution had reached 25 °C (Fig. 16, for full spectra, see Figure ESI6).

The upfield shift of the OH signals cannot be fully explained, but tentatively the observed signals could originate from non-associated molecules while the self-assembled species are NMR silent. Upon heating the sample of gelator **4**, the OH signals observed at 35 and 45 °C unexpectedly shift downfield. At 55 °C, the OH signals split and shift upfield, and at 65 °C the OH signals obtain their lowest ppm values in the series. The OH signals move downfield upon cooling, which is the expected behavior when the OH groups start to form hydrogen bonds. Consequently, in the VT NMR experiments of gelator **4**, the spectra obtained at the same temperature look very different upon heating and cooling. It appears that 20 min for temperature stabilization is insufficient for the self-assembly system of gelator **4** to fully equilibrate. Gel formation and stabilization or equilibration in compound **4** thus appear slower than for compound **3**, although the underlying reason remains unclear at present. Despite the two gelator compounds being structurally

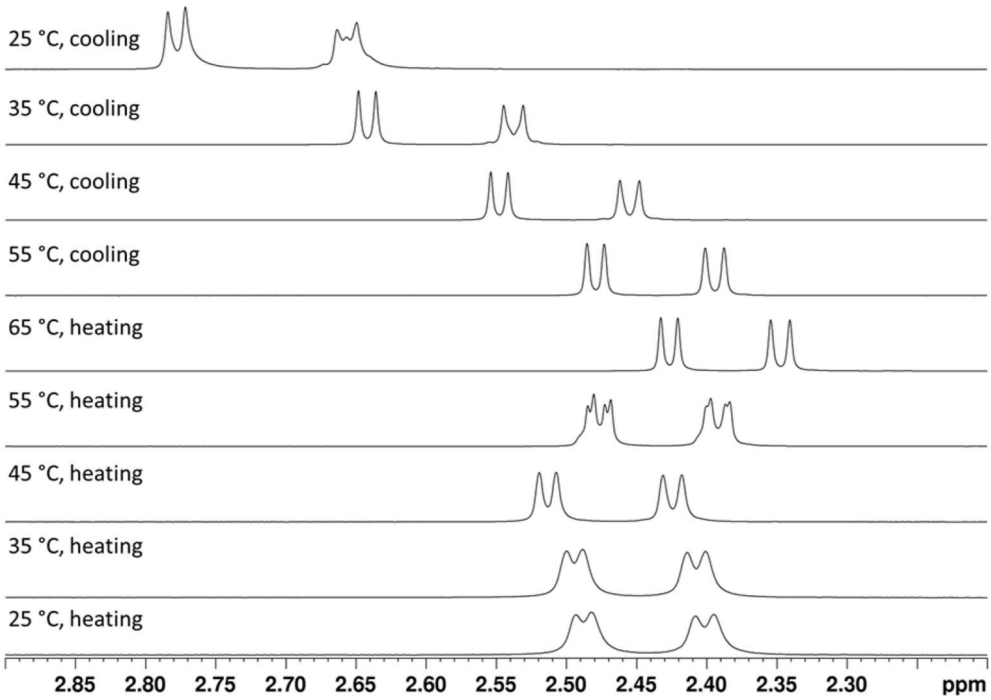

Fig. 16. Variable temperature ^{1}H NMR spectra (selected region for clarity) of compound **4** in decane-d_{22}.

very similar, the propyl end group of gelator **4** is more flexible than the allyl end group of gelator **3**, possibly causing a slower or more complex gel formation.

Solid state NMR spectroscopy is a complementary tool to X-ray crystallography for obtaining further structural information on crystalline solids, semisolids such as gels, and liquid crystals [52,53]. Cross polarization magic angle spinning (CP MAS) NMR experiments enable the study of gelator compounds in different forms, i.e., solid, xerogel, and even the native gel form [50]. Solid state NMR spectroscopy is an especially powerful tool for analyzing both xerogels and native gels. Similarities or deviations between the CP MAS NMR spectra of xerogels and native gels are sensitive to the morphological changes of the self-assembled network upon sample preparation (i.e., evaporation/-drying of the native gel). Previous studies have shown that the morphology of the native gel vs the xerogel may differ significantly [52]. In the present study, the ^{13}C CPMAS NMR spectra of the bulk powders, xerogels, and native gels derived from gelators **3** and **4** were compared. The solution state ^{13}C and ^{13}C CPMAS NMR spectra of the bulk form,

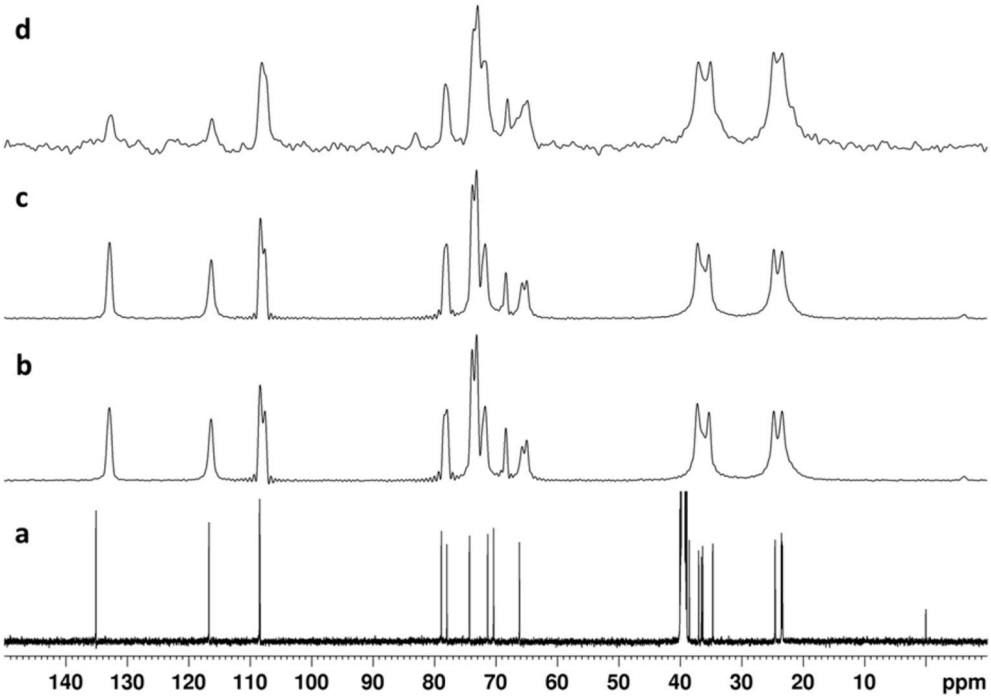

Fig. 17. ^{13}C NMR spectra of compound 3: a) Solution state ^{13}C NMR spectrum in DMSO-d_6; b) ^{13}C CPMAS NMR spectrum of the bulk powder; c) ^{13}C CPMAS NMR spectrum of the xerogel; d) ^{13}C CPMAS NMR spectrum of the native gel in decane-d_{22}.

xerogel and the native gel of gelator **3** are shown in Fig. 17.

By comparing the solution state ^{13}C NMR spectrum with the solid state spectrum of the bulk powder obtained from the non-gelating solvent ethyl acetate, it becomes evident that splitting of the signals in the carbohydrate region (60–80 ppm) occurs in the solid state spectrum of compound **3**, indicating the presence of more than one molecule in the asymmetric unit [54], which was additionally confirmed by single crystal X-ray and powder X-ray diffraction. The molecules in the asymmetric unit are non-equivalent in the magnetic environment and thus give rise to multiple sets of signals. Moreover, the solid state ^{13}C NMR spectral patterns of the bulk powder, xerogel and the native gel of compound **3** are identical, suggesting that the molecular packing in all three cases are similar, which was also confirmed by PXRD. The intensities of the allyl signals in the ^{13}C NMR spectrum obtained for the native gel are weaker, and the allyl signals are also slightly broader than in the bulk powder and xerogel spectral patterns. However, the broadening and low intensity might be a consequence of the unoptimized contact time of the pulse. The solid state NMR data for compound **4** shows similar trends, with splitting of the signals in the carbohydrate region, indicating more than one molecule in the asymmetric unit, and identical solid state spectra for the bulk powder, xerogel and native gel (Fig. 18).

3. Conclusion

In this work, potential low molecular weight organogelators derived from allylated D-mannose were prepared and analyzed. First, an alkene-terminated polyol compound bearing one cyclic ketal group and four free hydroxyls was tested. In this case, however, the hydrophilic/hydrophobic ratio proved too large and the compound did not gelate any of the tested solvents. Adding an additional ketal to the polyol backbone then resulted in phase-selective gelation of several different hydrocarbons and oils. The gels were thoroughly characterized by both solution state and solid state NMR spectroscopy, crystallographic methods, FTIR spectroscopy, rheometry, thermal microscopy and SEM. It could be concluded from FTIR spectroscopy, NMR analysis and X-ray crystallography that hydrogen bonding is the main driving force for self-assembly and gel formation, further demonstrating that the alkene moiety is not critical for gel formation. Thus, the alkene end-group remains available for further modifications, such as covalent or non-covalent binding to carrier materials or surfaces. This was further verified by preparation and analysis of a fully saturated analogue, which likewise phase-selectively formed gels with hydrocarbons. The gels formed by the saturated analogue showed similar properties as the gels derived from the allylated compound, but with slightly inferior mechanical strength. The gelators investigated require, however, heating in order to form gels, being currently impractical for large-scale applications, such as oil spill remediation. The solvent can, nevertheless, be easily recovered from the resulting gels and the gelator can be reused in multiple cycles. The gels formed are relatively weak, but future adsorption or covalent attachment to a carrier material could tentatively increase their mechanical strengths enabling applications where a tougher gel is required. In future work, hydrosilylation to silica gels or thiol-ene click reactions to thiol-functionalized surfaces, such as nanoparticles or cellulose, could potentially increase the mechanical strength and durability of the gels, increasing the number of potential applications. Further modifications and applications of the gelator compounds presented in this work remain to be investigated.

4. Experimental section

4.1. General considerations and gelator synthesis

All reagents and solvents were purchased from commercial vendors and were used without further purification. Allylated mannose and its hydrogenated congener were synthesized according to previously published protocols.[39] Compound **2** was prepared by dissolving allylated mannose (1 eq.) with *p*-TSOH (0.1 eq.) in dry DMF. Cyclohexanone dimethyl ketal (1.1 eq.) was added and the reaction was stirred at 60 °C at 200 mbar for 2 h. The reaction was quenched with triethylamine and the DMF was evaporated under reduced pressure. The formed mixture was purified by acetylation-chromatography-deacetylation cycle and the product was obtained as a white powder in 48% yield. Compounds **3** and **4** were synthesized by dissolving allylated mannose or the hydrogenated analogue (1 eq.) with *p*-TSOH (0.1 eq.) in dry DMF. Cyclohexanone dimethyl ketal (2.1 eq.) was added and the reaction was stirred at

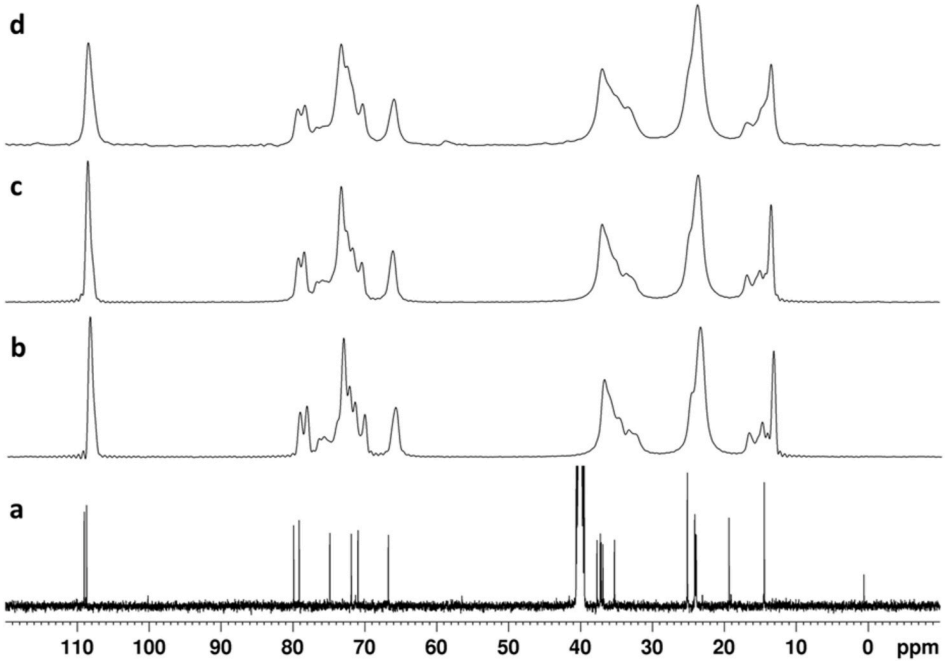

Fig. 18. ^{13}C NMR spectra of compound **4**: a) Solution state ^{13}C NMR spectrum in DMSO-d_6; b) ^{13}C CPMAS NMR spectrum of the bulk powder; c) ^{13}C CPMAS NMR spectrum of the xerogel. d) ^{13}C CPMAS NMR spectrum of the native gel in decane-d_{22}.

60 °C at 200 mbar for 2 h. The reaction was quenched with triethylamine and the DMF was evaporated under reduced pressure. The formed mixture was purified by column chromatography and the products were obtained as white powders in 43–46% yield. Further details and characterizations are found in ESI.

4.2. NMR spectroscopy

Solution state NMR spectra were recorded at 298 K on a Bruker Avance-III HD 500 MHz spectrometer equipped with a Bruker SmartProbe™. For characterization, DMSO-d_6 with 0.03% tetramethylsilane (TMS) as an internal standard was used as solvent. For gelation studies, decane-d_{22} was used as solvent. Coupling constants of solution state ^{1}H NMR spectra were solved with Chemadder/SpinAdder software, The Spin Discoveries Ltd [55]. CP MAS ^{13}C NMR spectra were obtained with a Bruker AVANCE-III HD 400 MHz spectrometer. Dry, powdered samples were spun at a 14 kHz spin rate in a Bruker ^{1}H broadband double-resonance 4 mm CP MAS probe. The native gels were spun at 5 kHz spin rate in a 30 μl Kel-F HR-MAS insert inside the 4 mm ZrO_2 rotor. The proton 90° high-power pulse was 2.9 μs, contact time 2 ms and the recovery delay time was set to 5 s. For dry samples, 8k scans were accumulated to obtain satisfactory signal-to-noise ratio, whereas 30k scans were acquired for the gel samples. Note: numbering in the NMR assignation of compounds **2**–**4** (see Scheme 1) does not match the numbering in the systematic name.

4.3. Gel formation

The gelation ability of compounds **2**–**4** in a series of organic solvents was investigated by dissolving the gelator (2% w/v, mg/ml) in the corresponding solvent by gentle heating (if soluble). In order to determine the minimum gelation concentration (MGC), small aliquots of solvent were added and the gelation procedure was repeated until the gel was no longer able to retain all of the solvent upon inversion. Likewise, the T_{gel} was determined by the inversion method for 2% w/v gel samples. The gels were slowly heated and the temperature when the sample could no longer withstand inversion was denoted as the T_{gel}.

4.4. Rheological studies

The rheological studies were conducted with a TA Instruments AR 2000ex rheometer with 8 mm parallel plate geometry. Gels of 5% w/v concentration were prepared and allowed to set for 2 h. The sample was placed on the sample surface of the rheometer and experiments were conducted both in frequency sweep and amplitude sweep modes. The frequency sweep experiments were conducted with 0.5% strain from 1 to 100 Hz. Amplitude sweep experiments were conducted at 1 Hz with amplitude range from 1.0×10^{-5} to 0.08 rad.

4.5. X-ray crystallography

Single crystal analyses of compounds **3** and **4** were made using a dual source (Cu/Mo) Agilent SuperNova diffractometer equipped with multilayer optics for generating monochromatized Cu K_α radiation (λ = 1.5418 Å), and Atlas CCD detector for recording data. Compound **3** crystallized as small bundles of tiny needles, whereas compound **4** crystallized as long, extremely narrow, twinned needles. For a measurement a crystal was mounted in a MiTeGen MicroMount™ loop (100 μm), and data collection was made under N_2 stream at −153 °C. Data collection (strategy included collection of Friedel pairs), reduction and analytical numeric absorption corrections by multifaceted crystal models were all made using CrysAlisPRO program (v. 41.112a) [56]. The crystal structure was solved with SHELXT [57] and refined on F^2 by full matrix least squares techniques with ShelXL [58] program both implemented in Olex^2 (v. 1.5) program package [59]. All non-hydrogen atoms were refined with anisotropic displacement parameters. All C–H hydrogens were calculated into their ideal positions using isotropic displacement parameters 1.2 times of the host atom. All hydroxyl group and allyl group hydrogens were located on a difference Fourier map in case of compound **3** and were refined without constraints. Despite of several structure determination attempts, only extremely poor data was acquired for compound **4** and, due to the low data quality, all hydrogen atoms of the structure were calculated to their ideal positions with proper riding model using isotropic displacement factors. The lack of heavier scatterers and data quality prevented the assignment of absolute configuration. Therefore, the handedness of the structures were set based on the synthesis reference of the starting molecule (D-mannose). Atom site occupancies on disorder model of the cyclohexanone ketal groups were first refined but as those settled close to 0.50, all disorder occupancies were fixed to 0.50 in the final refinement.

4.6. Powder X-ray diffraction

Powder X-ray diffraction data of compounds **3** and **4** were measured using PANalytical X'Pert Pro MPD diffractometer in Bragg-Brentano geometry using sealed X-ray tube generated Cu K_α (λ = 1.5418 Å) radiation and position-sensitive X'Celerator detector. Each sample was attached on a silicon-made "zero-background signal generating" disc using petrolatum jelly as an adhesive. Diffraction data were recorded at room temperature with 2θ-range of 3–60°, a step size of 0.017° and counting times of 120 s per step. Native gel samples were prepared to steel-made disc with sample cavity (16 mmm diameter, 2.5 mm depth). Data processing and search-match phase analyses were made using program X'pert HighScore Plus (v. 4.9). To compare the structural properties between the single crystals and bulk powders, the unit cell parameters of the powder samples were refined using Pawley method. The corresponding single crystal structure parameters were used as the basis of least-square refinements. Refined variables were as follows: background parameters, zero-offset, sample displacement, unit cell and peak profile parameters including peak width, shape and asymmetry parameters.

4.7. Other characterization methods

SEM images were obtained with a LEO Gemini 1530 instrument equipped with a Thermo Scientific UltraDry Silicon Drift Detector (SDD). The samples were sputtered with Pd prior to analysis. FTIR-ATR spectra were collected with a ThermoScientific Nicolet iS50 ATR instrument. The thermal microscope images were obtained by OLYMPUS BX51 stereo microscope equipped with OLYMPUS DP-23 high-resolution color CCD-camera, OLYMPUS cellSens imaging software and Linkam LTS420 hostage. HRMS were recorded with a Bruker Daltonics micro-QToF instrument in positive mode using ESI-ionization. Optical rotations were measured on a PerkinElmer 241 digital polarimeter with a 1 dm, 1 ml cell. Melting points were measured using a Stuart Scientific melting point apparatus.

Declaration of competing interest

The authors declare that they have no known competing financial interests or personal relationships that could have appeared to influence the work reported in this paper.

Acknowledgements

IM gratefully acknowledges the Society of Swedish Literature in Finland for funding. Dr. Jani Rahkila is thanked for valuable help with the NMR experiments. Linus Silvander is acknowledged for SEM-analysis. Dr. Mohammad Khajeheian and Rajesh Koppolu are thanked for rheology measurements and for assisting with data interpretation. Lucas Lagerquist and Dr. Jan-Erik Lönnqvist are thanked for assistance with additional chemical analysis.

Supplementary data

Complete crystallographic data for the structural analysis have been deposited with the Cambridge Crystallographic Data Centre, CCDC no. 2149491 (compound 3) and 2149492 (compound 4). Copies of this information may be obtained free of charge from the Director, Cambridge Crystallographic Data Centre, 12 Union Road, Cambridge, CB2 1EZ, UK. (fax: +44-1223-336033, e-mail: deposit@ccdc.cam.ac.uk or via: www.ccdc.cam.ac.uk).

Appendix A. Supplementary data

Supplementary data to this article can be found online at https://doi.org/10.1016/j.carres.2022.108596.

References

[1] A. Prathap, K.M. Sureshan, Sugar-based organogelators for various applications, Langmuir 3 (2019) 6005–6014, https://doi.org/10.1021/acs.langmuir.9b00506.

[2] A. Wynne, M. Whitefield, A.J. Dixon, S. Anderson, An effective, cosmetically acceptable, novel hydro-gel emollient for the management of dry skin conditions, J. Dermatol. Treat. 13 (2002) 61–66, https://doi.org/10.1080/09546630231758440 3.

[3] R.M. Martinez, C. Rosado, M.V. R Velasco, S.C.S. Lannes, A.R. Baby, Main features and applications of organogels in cosmetics, Int. J. Cosmet. Sci. 41 (2019) 109–117, https://doi.org/10.1111/ics.12519.

[4] K.Y. Lee, D.J. Mooney, Hydrogels for tissue engineering, Chem. Rev. 101 (2001) 1869–1880, https://doi.org/10.1021/cr000108x.

[5] Z. Yang, G. Liang, L. Wang, B. Xu, Using a kinase/phosphatase switch to regulate a supramolecular hydrogel and forming the supramolecular hydrogel in vivo, J. Am. Chem. Soc. 128 (2006) 3038–3043, https://doi.org/10.1021/ja057412y.

[6] S. Sahoo, N. Kumar, N.C. Bhattacharya, S.S. Sagiri, K. Jain, K. Pal, S.S. Ray, B. Nayak, Organogels: properties and applications in drug delivery, des, Monomers Polym 14 (2011) 95–108, https://doi.org/10.1163/138577211X555721.

[7] J.J.D. de Jong, L.N. Lucas, R.M. Kellogg, J.H. van Esch, B.L. Feringa, Reversible optical transcription of supramolecular chirality into molecular chirality, Science 304 (2004) 278–281, https://doi.org/10.1126/science.1095353.

[8] K. Murata, M. Aoki, T. Nishi, A. Ikeda, S.J. Shinkai, New cholesterol-based gelators with light- and metal-responsive functions, Chem. Soc. Chem. Commun. 24 (1991) 1715–1718, https://doi.org/10.1039/C39910001715.

[9] P. Xue, R. Lu, G. Chen, Y. Zhang, H. Nomoto, M. Takafuji, H. Ihara, Functional organogel based on a salicylideneaniline derivative with enhanced fluorescence emission and photochromism, Chem. Eur J. 13 (2007) 8231–8239, https://doi.org/10.1002/chem.200700321.

[10] A. Vidyasagar, K. Handore, K. M Sureshan, Soft optical devices from self-healing gels formed by oil and sugar-based organogelators, Angew. Chem. Int. Ed. 50 (2011) 8021–8024, https://doi.org/10.1002/anie.201103584.

[11] A. Ajayaghosh, V.K. Praveen, C. Vijayakumar, Organogels as scaffolds for excitation energy transfer and light harvesting, Chem. Soc. Rev. 37 (2008) 109–122, https://doi.org/10.1039/B704456A.

[12] S. Bhattacharya, Y. Krishnan-Ghosh, First report of phase selective gelation of oil from oil/water mixtures. Possible implications toward containing oil spills, Chem. Commun. 2 (2001) 85–186, https://doi.org/10.1039/B007848O.

[13] S. Bhattacharya, A. Pal, Physical gelation of binary mixtures of hydrocarbons mediated by N-Lauroyl-l-Alanine and characterization of their thermal and mechanical properties, J. Phys. Chem. B 112 (2008) 4918–4927, https://doi.org/10.1021/jp7104715.

[14] S. Debnath, A. Shome, S. Dutta, P.K. Das, Dipeptide-based low-molecular-weight efficient organogelators and their application in water purification, Chem. Eur J. 14 (2008) 6870–6881, https://doi.org/10.1002/chem.200800731.

[15] B.O. Okesola, D.K. Smith, Applying low-molecular weight supramolecular gelators in an environmental setting – self- assembled gels as smart materials for pollutant removal, Chem. Soc. Rev. 45 (2016) 4226–4251, https://doi.org/10.1039/C6CS00124F.

[16] N.M. Sangeetha, U. Maitra, Supramolecular gels: functions and uses, Chem. Soc. Rev. 34 (2005) 821–836, https://doi.org/10.1039/B417081B.

[17] P. Terech, R.G. Weiss, Low molecular mass gelators of organic liquids and the properties of their gels, Chem. Rev. 97 (1997) 3133–3160, https://doi.org/10.1021/cr9700282.

[18] O. Gronwald, E. Snip, S. Shinkai, Gelators for organic liquids based on self-assembly: a new facet of supramolecular and combinatorial chemistry, Curr. Opin. Colloid Interface Sci. 7 (2002) 148–156, https://doi.org/10.1016/S1359-0294(02)00016-X.

[19] K.B. Pal, B. Mukhopadhyay, Carbohydrate-based safe fuel gel with significant self–healing property, ChemistrySelect 2 (2017) 967–974, https://doi.org/10.1002/slct.201601776.

[20] N. Basu, A. Chakraborty, R. Ghosh, Carbohydrate derived organogelators and the corresponding functional gels developed in recent time, Gels 4 (2018) 52, https://doi.org/10.3390/gels4020052.

[21] C.-W. Chu, C.A. Schalley, Recent advances on supramolecular gels: from stimuli-responsive gels to Co-assembled and self-sorted systems, Org. Mater. 3 (2021) 25–40, https://doi.org/10.1055/s-0040-1722263.

[22] O. Gronwald, S. Shinkai, Sugar-integrated gelators of organic solvents, Chem. Eur J. 7 (2001) 4328–4334, https://doi.org/10.1002/1521-3765(20011015)7:20<4328::AID-CHEM4328>3.0.CO;2-S.

[23] R.J.H. Hafkamp, M.C. Feiters, R.J.M. Nolte, Organogels from carbohydrate amphiphiles, J. Org. Chem. 64 (1999) 412–426, https://doi.org/10.1021/jo981158t.

[24] S.R. Jadhav, P.K. Vemula, R. Kumar, S.R. Raghavan, G. John, Sugar-derived phase-selective molecular gelators as model solidifiers for oil spills, Angew. Chem. Int. Ed. 49 (2010) 7695–7698, https://doi.org/10.1002/anie.201002095.

[25] C.S. Kesava Raju, B. Pramanik, R. Ravishankar, P.V. Chalapathi Rao, G. Sriganesh, Xylitol based phase selective organogelators for potential oil spillage recovery, RSC Adv. 7 (2017) 37175–37180, https://doi.org/10.1039/C7RA06898K.

[26] S. Mukherjee, B. Mukhopadhyay, Phase selective carbohydrate gelator, RSC Adv. 2 (2012) 2270–2273, https://doi.org/10.1039/C2RA00036A.

[27] S. Mukherjee, G. Rama Krishna, B. Mukhopadhyay, C.A. Malla Reddy, A correlation study between hydrogen-bonded network and gelation ability of three galactose derivatives, CrystEngComm 17 (2015) 3345–3353, https://doi.org/10.1039/C5CE00229J.

[28] A. Mitra, V. Sarkar, B. Mukhopadhyay, Simple carbohydrate-derived multifunctional gels, ChemistrySelect 2 (2017) 9958–9961, https://doi.org/10.1002/slct.201701495.

[29] Rajkamal, D. Chatterjee, A. Paul, S. Banerjee, S. Yadav, Enantiomeric organogelators from D-/l-Arabinose for phase selective gelation of crude oil and their gel as a photochemical micro-reactor, Chem. Commun. 50 (2014) 12131–12134, https://doi.org/10.1039/C4CC05950F.

[30] N. P. Pathak Rajkamal, D. Chatterjee, A. Paul, S. Yadav, Arabinose based gelators: rheological characterization of the gels and phase selective organogelation of crude-oil, RSC Adv. 6 (2016) 92225–92234, https://doi.org/10.1039/C6RA21109G.

[31] S. Roy, A. Chakraborty, R. Ghosh, Aryl 4,6-O-Arylidene-1-Thio-β-d-Glycopyranoside-Based new organogelators and their gels, Carbohydr. Res. 343 (2008) 2523–2529, https://doi.org/10.1016/j.carres.2008.06.005.

[32] M. Samateh, A. Vidyasagar, S.R. Jadhav, G. John, Sugar based amphiphiles: easily accessible and efficient crude oil spill thickening agents, RSC Adv. 6 (2016) 107598–107605, https://doi.org/10.1039/C6RA21871G.

[33] W. Chen, Y. Yang, C.H. Lee, A.Q. Shen, Confinement effects on the self-assembly of 1,3:2,4-Di-p-Methylbenzylidene sorbitol based organogel, Langmuir 24 (2008) 10432–10436, https://doi.org/10.1021/la801734x.

[34] S. Grassi, E. Carretti, L. Dei, C.W. Branham, B. Kahr, R.G. Weiss, D-Sorbitol, A structurally simple, low molecular-mass gelator, New J. Chem. 35 (2011) 445–452, https://doi.org/10.1039/C0NJ00673D.

[35] S. Mukherjee, C. Shang, X. Chen, X. Chang, K. Liu, C. Yu, Y. Fang, N-Acetylglucosamine-Based efficient, phase-selective organogelators for oil spill remediation, Chem. Commun. 50 (2014) 13940–13943, https://doi.org/10.1039/C4CC06024E.

[36] A.M. Vibhute, V. Muvvala, K.M. Sureshan, Sugar-based gelator for marine oil-spill recovery, Angew. Chem. Int. Ed. 55 (2016) 7782–7785, https://doi.org/10.1002/anie.201510308.

[37] A. Prathap, K.M. Sureshan, A mannitol based phase selective supergelator offers a simple, viable and greener method to combat marine oil spills, Chem. Commun. 48 (2012) 5250–5252, https://doi.org/10.1039/C2CC31631E.

[38] T. Saloranta, A. Peuronen, J.M. Dieterich, J. Ruokolainen, M. Lahtinen, R. Leino, From mannose to small amphiphilic polyol: perfect linearity leads to spontaneous aggregation, Cryst. Growth Des. 16 (2016) 655–661, https://doi.org/10.1021/acs.cgd.5b01135.

[39] I. Mattsson, M. Lahtinen, A. Peuronen, A. Sau, A. Gunell, T. Saloranta-Simell, R. Leino, Thermal, spectroscopic, and crystallographic analysis of mannose-derived linear polyols, Cryst. Growth Des. 18 (2018) 3151–3160, https://doi.org/10.1021/acs.cgd.8b00263.

[40] S. Ikeda, K.J. Nishinari, Weak gel"-type rheological properties of aqueous dispersions of nonaggregated κ-carrageenan helices, J. Agric. Food Chem. 49 (2001) 4436–4441, https://doi.org/10.1021/jf0103065.

[41] K. Almdal, J. Dyre, S. Hvidt, O. Kramer, Towards a phenomenological definition of the term 'gel.', polym, Gels Networks 1 (1993) 5–17, https://doi.org/10.1016/0966-7822(93)90020-I.

[42] A. Prathap, K.M. Sureshan, Organogelator–cellulose composite for practical and eco-friendly marine oil-spill recovery, Angew. Chem. Int. Ed. 56 (2017) 9405–9409, https://doi.org/10.1002/anie.201704699.

[43] K. Yoza, N. Amanokura, Y. Ono, T. Akao, H. Shinmori, M. Takeuchi, S. Shinkai, D. N. Reinhoudt, Sugar-integrated gelators of organic solvents—their remarkable diversity in gelation ability and aggregate structure, Chem. Eur J. 5 (1999) 2722–2729, https://doi.org/10.1002/(SICI)1521-3765(19990903)5:9<2722::AID-CHEM2722>3.0.CO;2-N.

[44] J.H. Jung, S. Shinkai, T. Shimizu, Spectral characterization of self-assemblies of aldopyranoside amphiphilic gelators: what is the essential structural difference between simple amphiphiles and bolaamphiphiles? Chem. Eur J. 8 (2002) 2684–2690, https://doi.org/10.1002/1521-3765(20020617)8:12<2684::AID-CHEM2684>3.0.CO;2-Z.

[45] B. Escuder, M. LLusar, J.F. Miravet, Insight on the NMR study of supramolecular gels and its application to monitor molecular recognition on self-assembled fibers, J. Org. Chem. 71 (2006) 7747–7752, https://doi.org/10.1021/jo0612731.

[46] A.R. Hirst, I.A. Coates, T.R. Boucheteau, J.F. Miravet, B. Escuder, V. Castelletto, I. W. Hamley, D.K. Smith, Low-molecular-weight gelators: elucidating the principles

of gelation based on gelator solubility and a cooperative self-assembly model, J. Am. Chem. Soc. 130 (2008) 9113–9121, https://doi.org/10.1021/ja801804c.
[47] F. Allix, P. Curcio, Q.N. Pham, G. Pickaert, B. Jamart-Grégoire, Evidence of intercolumnar Π−π stacking interactions in amino-acid-based low-molecular-weight organogels, Langmuir 26 (2010) 16818–16827, https://doi.org/10.1021/la102864y.
[48] P. Terech, A. Coutin, A.M. Giroud-Godquin, Scattering of a crystalline gel network: a new organogel based upon a benzohydroxamic acid derivative, J. Phys. Chem. B 101 (1997) 6810–6818, https://doi.org/10.1021/jp970371a.
[49] K. Sakurai, Y. Jeong, K. Koumoto, A. Friggeri, O. Gronwald, S. Sakurai, S. Okamoto, K. Inoue, S. Shinkai, Supramolecular structure of a sugar-appended organogelator explored with synchrotron X-ray small-angle scattering, Langmuir 19 (2003) 8211–8217, https://doi.org/10.1021/la0346752.
[50] H. Svobodová, Nonappa, Z. Wimmer, E. Kolehmainen, Design, synthesis and stimuli responsive gelation of novel stigmasterol–amino acid conjugates, J. Colloid Interface Sci. 361 (2011) 587–593, https://doi.org/10.1016/j.jcis.2011.05.084.
[51] E. Snip, S. Shinkai, D.N. Reinhoudt, Organogels of a nucleobase-bearing gelator and the remarkable effects of nucleoside derivatives and a porphyrin derivative on the gel stability, Tetrahedron Lett. 42 (2001) 2153–2156, https://doi.org/10.1016/S0040-4039(01)00095-8.
[52] Nonappa, E. Kolehmainen, Solid state NMR studies of gels derived from low molecular mass gelators, Soft Matter 12 (2016) 6015–6026, https://doi.org/10.1039/C6SM00969G.
[53] M. El Hariri El Nokab, P.C.A. van der Wel, Use of solid-state NMR spectroscopy for investigating polysaccharide-based hydrogels: a review, Carbohydr. Polym. 240 (2020) 116276, https://doi.org/10.1016/j.carbpol.2020.116276.
[54] Nonappa, M. Lahtinen, B. Behera, E. Kolehmainen, U. Maitra, Unraveling the packing pattern leading to gelation using SS NMR and X-ray diffraction: direct observation of the evolution of self-assembled fibers, Soft Matter 6 (2010) 1748–1757, https://doi.org/10.1039/B919619F.
[55] ChemAdder/Spinadder, Spin Discoveries Ltd.
[56] CrysAlisPro Software System, Rigaku Corporation, Oxford, 2019.
[57] G.M. Sheldrick, \it SHELXT} {–} integrated space-group and crystal-structure determination, Acta Crystallogr. A 71 (2015) 3–8, https://doi.org/10.1107/S2053273314026370.
[58] G.M. Sheldrick, Acta Crystallogr. C 71 (2015) 3–8, https://doi.org/10.1107/S2053229614024218.
[59] O.V. Dolomanov, L.J. Bourhis, R.J. Gildea, J.A.K. Howard, H. Puschmann, {\it OLEX2}: a complete structure solution, refinement and analysis program, J. Appl. Crystallogr. 42 (2009) 339–341, https://doi.org/10.1107/S0021889808042726.